

Hydrothermal synthesis of hemisphere-like F-doped anatase TiO₂ with visible light photocatalytic activity

Changlin Yu · Wanqin Zhou · Kai Yang · Gan Rong

Received: 18 March 2010/Accepted: 21 May 2010/Published online: 5 June 2010
© Springer Science+Business Media, LLC 2010

Abstract Hemisphere-like F-doped anatase TiO₂ has been synthesized by hydrothermal treatment of TiF₄ aqueous solution in the presence of starch at 130 °C for 10 h, and then calcined at 450 °C for 2.5 h in air. The as-synthesized product has been investigated by photocatalytic reaction test and characterized by powder X-ray diffraction (XRD), scanning electron microscopy (SEM), transmission electron microscopy (TEM), energy-dispersive X-ray (EDX) spectroscopy, X-ray photoelectron spectroscopy (XPS), and UV–Vis diffuse reflectance spectra (DRS). The results showed that fluorine was successfully doped into the TiO₂ hemispheres. The F-doped TiO₂ hemispheres showed high visible light activity in degradation of acid orange II, which could be attributed to the creation of oxygen vacancies and good crystallinity.

Introduction

Nowadays, semiconductor photocatalysts have been attached importance due to their applications to environmental purification and solar energy conversion [1–9]. Among photocatalysts, TiO₂ has received the most attention as a photocatalytic material because of its superior photocatalytic activity, chemical stability, low cost, and

nontoxicity [10, 11]. A major drawback of TiO₂ is the large band gap of 3.2 eV, and so the wavelengths below 400 nm are necessary for excitation, and only the small UV fraction of solar light, about 2–3%, can be utilized, which limits its effective application of solar energy. Many approaches have been developed to overcome this limitation. For example, the modification of semiconductors [12, 13], addition of transition metals [14, 15], and nonmetal doping [16, 17] are the common methods for the fabrication of visible light response catalysts. Among nonmetal dopings, fluorine doping has been found not only to promote the activity of TiO₂ by slowing down the radiative recombination process of photogenerated electrons and holes [1, 18–21] but also to induce a visible-light-driven photocatalysis by the creation of oxygen vacancies [22, 23].

On the other hand, due to the photocatalytic performance of the TiO₂ strongly depending on its size, shape, composition, and crystallinity, various nanostructures have been synthesized. To this end, a great deal of effort has been devoted to the synthesis of TiO₂ nanotubes, nanorods, nanowires, or shuttle-shape nanocrystals [24–26]. Recently, the fabrication of TiO₂ microspheres has been receiving much attention because of their low density, high surface area, delivering ability, and surface permeability [27, 28]. More recently, it has been reported that the hollow TiO₂ hemispheres could provide the enhanced photo-conversion efficiency with the uniquely geometric effect of the hollow microstructures [29, 30]. For photocatalysts, the high-energy conversion efficiencies as well as large light-harvesting capacities can be achieved by constructing their complex architectures. Till now, there are comparatively few reports about the fabrication of well-crystallized TiO₂ hemispheres. In this study, we designed a simple approach to generate hemisphere-like F-doped anatase TiO₂ using TiF₄ and starch as the precursors. A high visible light

C. Yu (✉) · K. Yang · G. Rong
School of Materials and Chemical Engineering, Jiangxi
University of Science and Technology, 86 Hongqi Road,
Ganzhou 341000, Jiangxi, China
e-mail: yuchanglinjx@163.com

W. Zhou
School of Information Engineering, Jiangxi University
of Science and Technology, 86 Hongqi Road,
Ganzhou 341000, Jiangxi, China

photocatalytic performance was obtained over these hemispheres.

Experimental

Synthesis of the samples

In a typical synthesis, 0.25 g of TiF_4 and 2 g of starch were dissolved in 30 mL deionized (DI) water. The solution was placed in a Teflon-lined stainless steel autoclave and maintained at 130 °C for 10 h. The black powders were collected by centrifugation, washed two times with DI water, and dried in an oven at 100 °C. Finally, the sample was placed in a furnace, and the temperature was raised up to 450 °C with a heating rate of 2 °C/min. The calcined time is 2.5 h.

Characterization of the samples

The XRD patterns, obtained on a Bruker D8 Advance X-ray diffractometer using $\text{CuK}\alpha$ radiation at a scan rate of 0.05° (2θ) s^{-1} , were used to identify the phase constitution in the samples and their crystallite size. The accelerating voltage and the applied current were 40 kV and 40 mA, respectively. The general morphology of the products was characterized by scanning electron microscopy (SEM, LEO, 1450VP). The products were conductively coated with gold by sputtering for 30 s to minimize charging effects under SEM imaging conditions. Transmission electron microscopy (TEM) images were recorded on a CM-120 microscope (Philips, 120 kV), coupled with an energy-dispersive X-ray (EDX, Oxford Instrument) spectrometer. Samples were deposited on thin amorphous carbon films supported by copper grids from ultrasonically processed ethanol solutions of the products. The samples were also analyzed by X-ray photoelectron spectroscopy (XPS) on a PHI Quantum 2000 XPS System with a monochromatic AlKa source and a charge neutralizer. All the binding energies were referenced to the C1s peak at 284.8 eV of the surface adventitious carbon. UV–Vis diffuse reflectance spectra were achieved using a UV–Vis spectrophotometer (Cary 100 scan spectrophotometers, Varian). Absorption spectra were referenced to BaSO_4 .

Photocatalytic activity measurement

The photocatalytic activities of the samples were determined by measuring the degradation of acid orange II in an aqueous solution under visible light irradiation. In visible light activity test, a 300-W tungsten halogen lamp with a $\lambda < 420$ nm cutoff filter was used as visible light source. The photocatalyst (0.05 g) was suspended in 80-mL

aqueous solution of acid orange II with the concentration of $C_0 = 0.020$ g/L. Prior to light illumination, the suspension was strongly magnetically stirred for 40 min in the dark for adsorption/desorption equilibrium. The suspension was vigorously stirred with the photoreactor during the process, and the temperature of suspension was maintained at 22 °C by circulation of water through an external cooling coil. At given intervals of illumination, the sample of suspension was taken out and centrifuged. The clear upper layer solution was analyzed by a Milton Roy Spectronic 3000 Array spectrophotometer (New York, USA). The dye concentration was measured at $\lambda = 484$ nm, the maximum absorption wavelength for acid orange II.

Results and discussion

Morphology and crystallinity analysis

It was reported that carbon microspheres could be prepared from sucrose by a hydrothermal method [31]. In our case, the hydrothermal treatment of the starch also produced very good morphologic carbon microspheres with the size of 2–3 μm , as shown in Fig. 1a. The products of the hydrothermal treatment of TiF_4 aqueous solution in the presence of starch are the C/TiO_2 core–shell microspheres with the diameter of 2–3 μm , which was confirmed by removing the core of carbon and XRD test. From Fig. 1b, it can be seen that these C/TiO_2 core–shell microspheres have no smooth surface as that of pure carbon microspheres. The core of carbon was burnt off in the calcination process, and the quas-ordered hollow TiO_2 hemispheres were produced, as shown in Fig. 1c. High-resolution transmission electron microscopy (HRTEM) image, Fig. 1d, shows the TiO_2 hemispheres with well-defined structure. The interplanar distance is about 0.35 nm. This fringe spacing is a characteristic of the anatase crystal phase in the (101) plane. From the HRTEM image, the size of prime crystalline is estimated to be about 10 nm. Figure 2 is an EDX spectrum of the F-doped hemispheres. Five elements are shown. These elements are C, O, Ti, F, and Cu (the peaks of C and Cu come from the supporting copper grid with carbon films). These results confirmed that the F was introduced into TiO_2 hemispheres.

The phase composition and the crystallinity of the carbon microspheres, C/TiO_2 core–shell microspheres and TiO_2 hemispheres were determined by XRD test, and the results are shown in Fig. 3. The XRD pattern of the carbon microspheres shows that this carbon formed at this condition is amorphous. Over C/TiO_2 core–shell microspheres, four diffraction peaks at 2θ of 25.3, 38.2, 48.1, 53.5, and 55.6° appear. All of these peaks can be readily indexed to the pure anatase phase with lattice constants, $a = 3.7806$ Å

Fig. 1 **a** carbon microspheres; **b** C/TiO₂ core–shell microspheres; **c** TiO₂ hemispheres; **d** The fringes with a spacing of 0.35 nm correspond to (101) planes

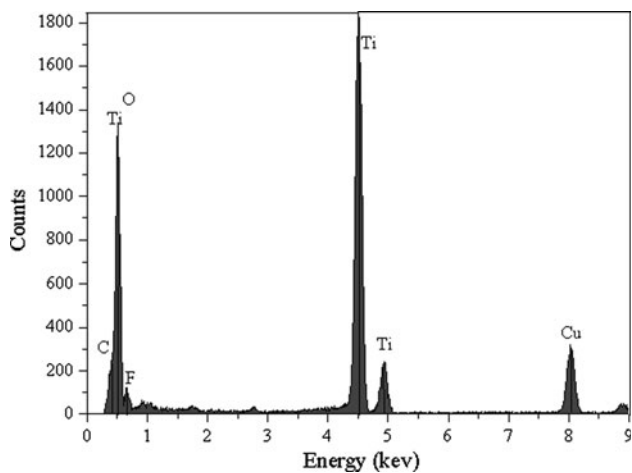
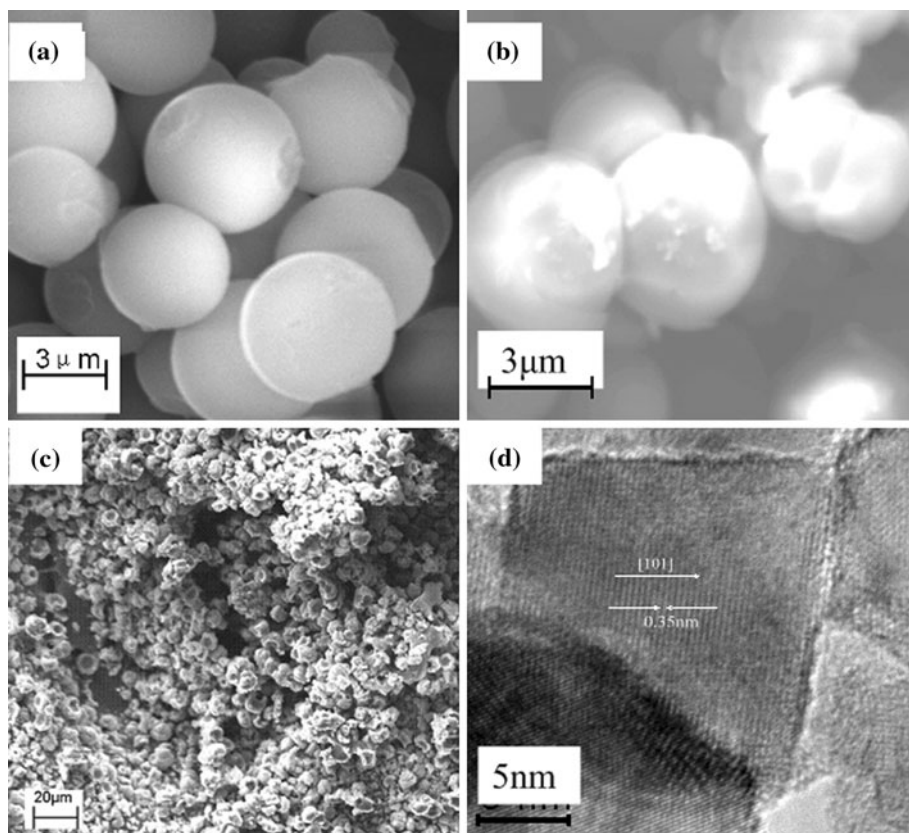


Fig. 2 EDX spectrum of the F-doped TiO₂ hemispheres

and $c = 9.4977 \text{ \AA}$, which are in agreement with the reported values (JCPDS No. 21-1272). Over TiO₂ hemispheres no characteristic peaks of other impurities are observed, which indicate that the product has high purity. The average crystallite sizes of the TiO₂ hemispheres were calculated according to the Scherrer's equation using the fwhm data of each phase after correcting the instrumental broadening. The prime crystalline size of TiO₂ is estimated to 10–13 nm which is almost consistent with the former TEM test.

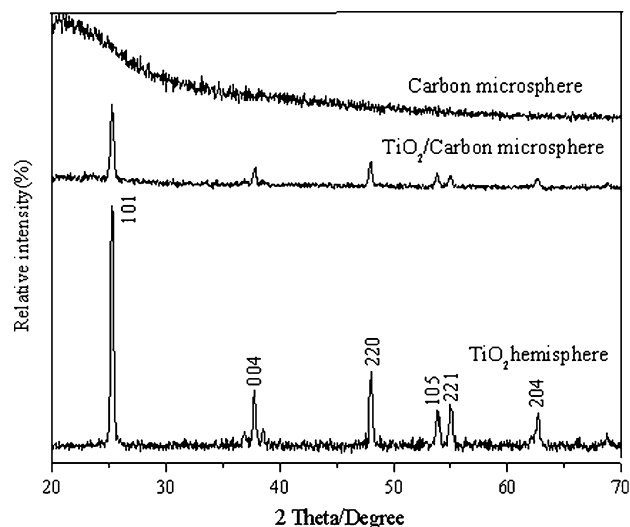
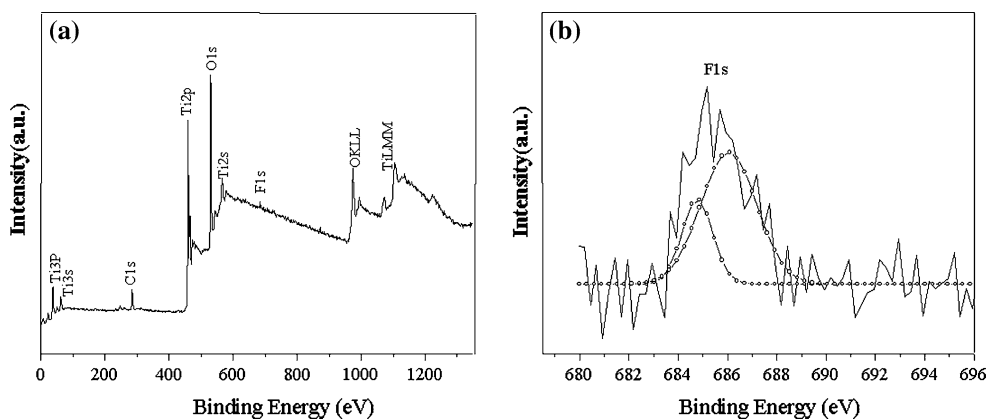


Fig. 3 XRD patterns of the synthesized carbon, TiO₂/carbon microspheres, and TiO₂ hemisphere

XPS-analysis

The elemental composition of the F-doped TiO₂ hemisphere was further determined by XPS. Fig. 4a shows that the prepared TiO₂ hemispheres consist of Ti, O, C, and F elements. The C element may mainly be ascribed to the adventitious hydrocarbon from XPS itself. The atomic ratio

Fig. 4 **a** The survey spectrum of F-doped TiO_2 hemispheres; and **b** F1s XPS spectra



of $\text{Ti}: \text{O}: \text{F}$ was estimated to be 1:2.12:0.018, which is in good agreement with the nominal atomic composition of TiO_2 . Figure 4b shows the high-resolution XPS spectra of F1s. The F1s peak can be deconvoluted into two peaks with Gaussian distributions, which indicates that two forms of F are present. Peak 1 located at around 684.8 eV could be attributed to the F atoms in TiOF_2 . However, it is reasonable to ascribe peak 2 to the substitutional F atoms in TiO_2 because the position of this peak (686.3 eV) is close to the value previously reported in the literatures [4, 18]. The substitutional F atoms could occupy oxygen sites in the TiO_2 crystal lattice and result in the appearance of oxygen vacancies. This confirms that F atoms were doped into the oxygen sites of the TiO_2 crystal lattice. It should be mentioned that when the -1 fluoride ions replace the -2 oxygen ions in the lattice, a charge imbalance is created. The extra positive charge is probably neutralized by the hydroxide ions by forming surface adsorbed hydroxyl groups [23].

UV–Vis diffuse reflectance spectra

Figure 5 shows the result of diffuse reflection spectra of the pure anatase TiO_2 and F-doped TiO_2 hemispheres. The pure anatase TiO_2 presents the photo-absorption properties in the UV light region at around 400 nm. Compared to the absorption spectra of pure anatase TiO_2 , F doping does not cause an obvious shift in the fundamental absorption edge of TiO_2 . This conclusion is consistent with the previous report in literature [23] and theoretical band calculations for F-doped TiO_2 reported by Asahi et al [32]. When TiO_2 is doped with fluorine, localized levels with high density appear below the valence band of TiO_2 . These levels consist of the F 2p state without any mixing with either the valence band or the conduction band of TiO_2 .

The mechanism for the formation of TiO_2 hemispheres

A simple model for the formation of TiO_2 hemispheres was suggested in Fig. 6. At the hydrothermal conditions, the

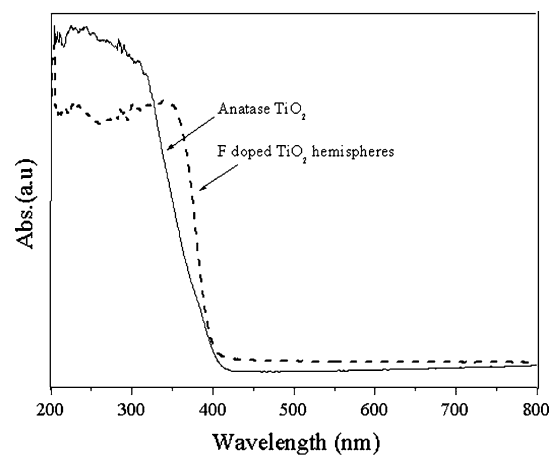


Fig. 5 UV–Vis diffuse reflectance spectra

starch is easy to be dehydrated and form the carbon microspheres. On the other hand, with time prolonging, TiF_4 slowly got hydrolyzed and formed colloidal Ti(OH)_4 . The hydrolysis reaction of TiF_4 could be expressed as the following equation: $\text{TiF}_4 + 2\text{H}_2\text{O} \rightarrow \text{Ti(OH)}_4 + 4\text{HF}$. The Ti^{4+} colloidal species was easily coated on the surface of carbon microsphere. Owing to the amorphous Ti^{4+} colloidal being in a thermodynamically metastable state, the species transforms to the stable crystalline state under hydrothermal conditions. Therefore, good crystalline TiO_2 was obtained under hydrothermal conditions. Most of the fluorine in TiF_4 was hydrolyzed and the residual fluorine would naturally remain as a dopant in the TiO_2 lattice. This phenomenon is similar to the situation of the conventional method in the synthesis of N-doped [33], S-doped [34], and C-doped TiO_2 [35] by oxidative annealing of TiN , TiS_2 , and TiC . In the process of calcination, the core of carbon was burnt off, and the TiO_2 /carbon microspheres were broken into the quasi-ordered TiO_2 hemispheres. The F doping may be further strengthened in calcination treatment. Our calcination experiments also showed that the mass ratio of starch to TiF_4 , the heating rate, and the calcination temperature are the key factors for the formation

Fig. 6 The model for the formation of TiO_2 hemispheres

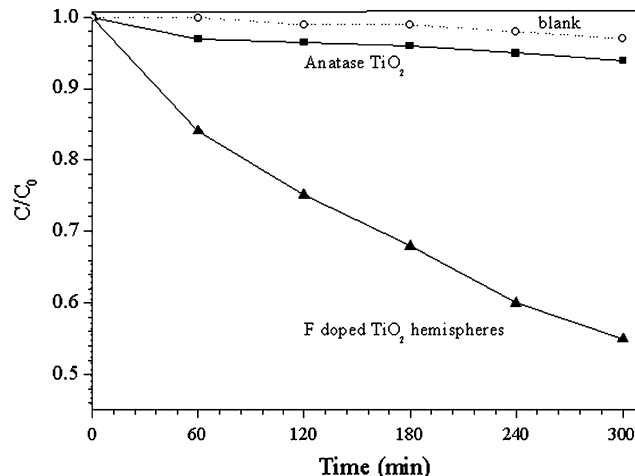
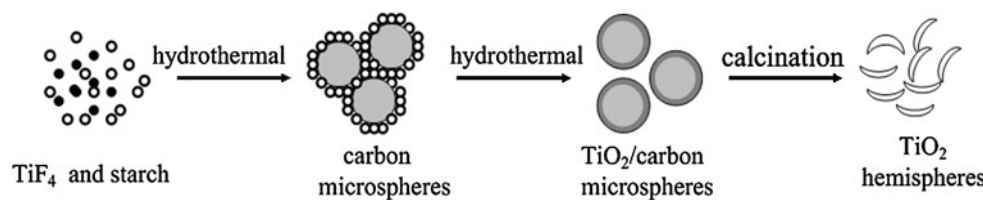


Fig. 7 Decomposition of acid orange II test under visible light irradiation

of TiO_2 hemispheres. The high ratio of starch to TiF_4 , high heating rate, and calcination temperature caused TiO_2 /carbon microspheres break into TiO_2 pieces, which mainly relates to the high production velocity of carbon dioxide. If a great deal of carbon dioxide was produced instantaneously, then TiO_2 /carbon microspheres are easy to break up and no regularly morphologic TiO_2 can be obtained.

Activity test of the F-doped TiO_2 hemispheres

The photocatalytic activities of the F-doped TiO_2 hemispheres and pure anatase TiO_2 were measured by degradation of acid orange II as a model reaction. Prior to irradiation, the dispersions were magnetically stirred in the dark for 40 min to achieve the adsorption/desorption equilibrium between TiO_2 and orange II. Figure 7 shows the acid orange II concentration changes under visible light ($\lambda > 420 \text{ nm}$) irradiation. It can be found that acid orange II almost cannot be degraded under visible light irradiation without catalysts, indicating that the photolysis of acid orange II can be ignored. The experimental data in the acid orange II decolorization with anatase TiO_2 as the catalyst shows that acid orange II almost cannot be degraded by pure TiO_2 . Surprisingly, the F-doped TiO_2 hemispheres are effective in the photocatalytic degradation of acid orange II under visible light illumination. It has been reported that the photoexcitation of extrinsic absorption bands of a catalyst can also lead to surface photoreactions [36]. It was

also reported by Yu [23] that the F-doped hierarchical TiO_2 spheres are very effective in the photocatalytic degradation of 4-chlorophenol under visible light illumination. In this study, the photocatalytic mechanism is similar to that described in Yu's article. As suggested in the literature [22], the high photocatalytic activity of F-doped TiO_2 hemispheres is probably due to the excitation of the extrinsic absorption bands by these oxygen vacancies rather than the excitation of the intrinsic absorption band of bulk TiO_2 because no obvious difference was observed on the UV–Vis diffuse reflectance spectra of the pure anatase TiO_2 and F-doped TiO_2 . The extrinsic absorption originates from the photoionization of original or newly formed defects, and the excitation of surface states. Such extrinsic absorption requires less energy to activate. Thus, it is possible to generate free charge carriers to induce surface chemical reactions by using visible light.

Conclusions

In summary, hemisphere-like F-doped anatase TiO_2 was fabricated by a simple hydrothermal combination with calcination method. The new photocatalysts show a high visible light photocatalytic activity on the degradation of acid orange II. The good crystallinity and the creation of oxygen vacancies by F doping could result in the high visible light photocatalytic activity.

Acknowledgements This work was supported by the Young Science Foundation of Jiangxi Province Education Office (GJJ10150), Open Foundation of State Key Laboratory of Physical Chemistry of Solid Surfaces, Xiamen University (200906), a fund for undergraduate innovation experiment of Jiangxi University of Science and Technology.

References

- Zhang J, Zhao DS, Wang JL, Yang LY (2009) *J Mater Sci* 44:3112. doi:[10.1007/s10853-009-3413-z](https://doi.org/10.1007/s10853-009-3413-z)
- Fallet M, Permpoon S, Deschanvres JL, Langlet M (2006) *J Mater Sci* 41:2915. doi:[10.1007/s10853-006-5077-2](https://doi.org/10.1007/s10853-006-5077-2)
- Dong SH, Xu KJ, Tian GS (2009) *J Mater Sci* 44:2548. doi:[10.1007/s10853-009-3332-z](https://doi.org/10.1007/s10853-009-3332-z)
- Yu CL, Yu JC, Chan M (2009) *J Solid State Chem* 182:1061
- Yu CL, Yu JC (2009) *Catal Lett* 129:462
- Lv XM, Xie JM, Song YZ, Lin JM (2007) *J Mater Sci* 42:6824. doi:[10.1007/s10853-006-1401-0](https://doi.org/10.1007/s10853-006-1401-0)

7. Yu CL, Yu JC (2009) *Mater Sci Eng B* 164:16
8. Yu CL, Yu JC (2010) *Mater Sci Eng B* 166:213
9. Ananpattarachai J, Kajitvichyanukul P, Seraphin S (2008) *J Hazard Mater* 152:48
10. Zhang J, Xu Q, Feng ZC, Li MJ, Li C (2008) *Angew Chem Int Ed* 47:1
11. Yu JC, Yu JG, Tang HY, Zhang LZ (2002) *J Mater Chem* 12:81
12. Zhang M, Chen CC, Ma WH, Zhao JC (2008) *Angew Chem Int Ed* 47:9730
13. Grätzel M (2003) *J Photochem Photobiol C: Photochem Rev* 4:145
14. Gong XQ, Selloni A, Dulub O, Jacobson P, Diebold U (2008) *J Am Chem Soc* 130:370
15. Rodrigues S, Ranjit KT, Uma S, Martyanov IN, Klabunde KJ (2005) *Adv Mater* 172:467
16. Liu G, Zhao YN, Sun CH, Li F, Lu GQ, Cheng HM (2008) *Angew Chem Int Ed* 47:1
17. Chen XF, Wang XC, Hou YD, Huang JH, Wu L, Fu XZ (2008) *J Catal* 255:59
18. Yu JC, Yu JG, Ho W, Jiang Z, Zhang L (2002) *Chem Mater* 14:3808
19. Ryu J, Choi W (2004) *Environ Sci Technol* 38:2928
20. Kim H, Choi W (2007) *Appl Catal B* 69:127
21. Wu GS, Chen AC (2008) *J Photochem Photobio A: Chem* 195:47
22. Li D, Haneda H, Labhsetwar NK, Hishita S, Ohashi N (2005) *Chem Phys Lett* 401:579
23. Ho WK, Yu JC, Lee SC (2006) *Chem Commun* 1115–1117
24. Macak JM, Tsuchiya H, Schmuki P (2005) *Angew Chem Int Ed* 44:2100
25. Jun YW, Casula MF, Sim JH, Kim SY, Cheon JW, Alivisatos AP (2003) *J Am Chem Soc* 125:15981
26. Kanie K, Sugimoto T (2004) *Chem Commun* 1584–1585
27. Li XX, Xiong YJ, Li ZQ, Xie Y (2006) *Inorg Chem* 45:3493
28. Li XZ, Liu H, Cheng LF, Tong HJ (2003) *Environ Sci Technol* 37:3989
29. Yu JG, Yu XX, Huang BB, Zhang XY, Dai Y (2009) *Cristal Growth Design* 9:1474
30. Yang SC, Yang DJ, Kim JK, JM Hong, Kim HG, Kim ID, Lee HJ (2008) *Adv Mater* 20:1059
31. Wang Q, Li H, Chen LQ, Huang XJ (2001) *Carbon* 39:2211
32. Asahi R, Morikawa T, Ohwaki T, Aoki K, Taga Y (2001) *Science* 293:269
33. Irie H, Washizuka S, Yoshino N, Hashimoto K (2003) *Chem Commun* 1298–1299
34. Yu JC, Ho WK, Yu JG, Yip HY, Wong PK, Zhao JC (2005) *Environ Sci Technol* 39:1175
35. Sakthivel S, Kisch (2003) *Angew Chem Int Ed* 42:4908
36. Emeline AV, Kuzmin GN, Purevdorj D, Ryabchuk VK, Serpone N (2000) *J Phys Chem B* 104:2989